Characterization of High-Strength Steel Weld Metals: Chemical Composition, Microstructure, and Nonmetallic Inclusions

General compositional and microstructural characteristics, including nonmetallic inclusions, of high-strength steel weld metals were studied

BY J. E. RAMIREZ

ABSTRACT. The use of high-strength steels (HSS) provides several potential advantages. However, the progress in steel technology continually demands new developments in welding processes and consumables to produce weld metals with mechanical properties equivalent to the base metal. To achieve this, however, a better understanding of chemistry- and microstructure-property relationships in HSS weld metals is needed. In this study, the general compositional and microstructural characteristics of HSS weld metals, including nonmetallic inclusions, were experimentally characterized. The weld metals were deposited using different welding processes and commercially available welding consumables with nominal strengths ranging from 490 to 840 MPa (70 to 120 ksi).

Introduction

The use of high-strength steels (HSS) provides several potential advantages including lower weight, lower manufacturing costs, and ease of handling and transport. Therefore, major impetus for developments in high-strength steels has been provided by the need for higher strength, increased toughness, and improved weldability. The development of HSS with better properties has been supported by improvements in the steelmaking industry for production of clean steels, the use of microalloying elements in combination with normalizing, controlled rolling or quenching, and tempering. Since 1982, the control of the steel properties through thermomechanical processing (TMCP) and accelerated cooling (AC) and/or direct quenching (DQ) have enabled steels to be produced with increased strength and toughness, while maintaining good weldability (Ref. 1).

HSSs with yield strengths of 450 MPa (X70) and 550 MPa (X80) are increasingly specified for use in different structural applications, resulting in weight and cost savings through the use of thinner sections. The use of X80 pipeline steels has become common in Canada (Ref. 2) and parts of Europe (Ref. 3). Additional refinement of chemical composition and processing procedures resulted in the development of higher-strength X100 steel in the early and mid-1990s (Ref. 4). Laboratory- and full-scale testing of X100 pipe and seam welds have recently been reported (Ref. 5). These studies suggest that with some refinement of the steelmaking procedures, target X100 properties can be achieved, and successful results of experimental work on X120 have been reported.

The progress in steel manufacturing technology has continually called for new developments in welding processes and consumables to produce weld metal deposits with mechanical properties essentially equivalent to the base metal. To achieve this, however, proper control of numerous factors that interact during welding to produce a weld metal with a certain chemical composition and a particular microstructure with characteristic properties is required. Additionally, it has been established that some high-strength weld metals exhibit a high degree of variability in mechanical property test results. The variability of the properties of a weld metal could come from various sources such as consumable lot-to-lot variation, procedural variation, positional variation, and base material variation. Sometimes chemical composition variations may explain the differences, but in many cases, they do not. It is clear that a better understanding of chemistry- and microstructure-property relationships in HSS weld metals is needed.

The main objective of this study was to experimentally characterize the general compositional and microstructural characteristics of HSS weld metals, including nonmetallic inclusions. In an attempt to cover a broad range of applications normally found in different industries, the weld metals were deposited using different welding processes and commercially available welding consumables with nominal tensile strengths ranging from 490 to 840 MPa (70 to 120 ksi). Applications for these welding consumables would include welding of API 5L pipeline steels such as X70, X80, and X100, as well as plate steels and structural shapes of similar strength levels.

KEYWORDS

High-Strength Steels (HSS)
Weld Metals
Nonmetallic Inclusions
FCAW
SMAW
GMAW

Experimental Procedures

The characterization of the weld metals deposited with different welding processes and consumables included chemical composition, microstructural analysis, and evaluation of nonmetallic inclusions. Details regarding the materials and experimental procedures are summarized as follows.

Base Metals

Different materials ranging from low-strength A-36 steel plates to high-strength X80 pipe steels and X100 steel plates were used as base materials for this study, as

J. E. RAMIREZ (jose_ramirez@ewi.org) *is a principal engineer with the Edison Welding Institute, Columbus, Ohio.*

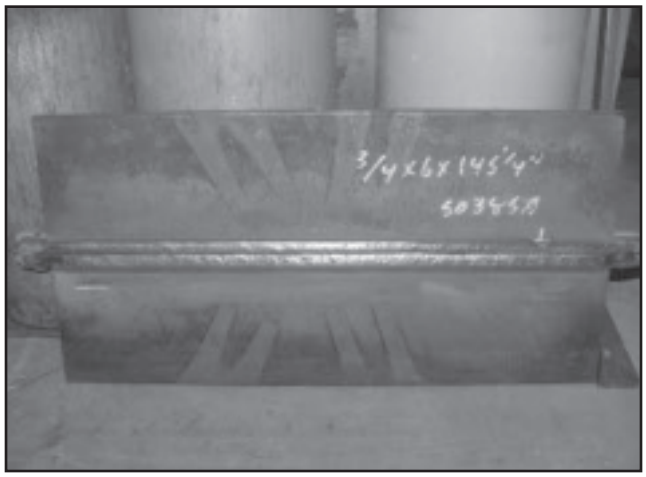

Fig. 1 — General view of welded joint.

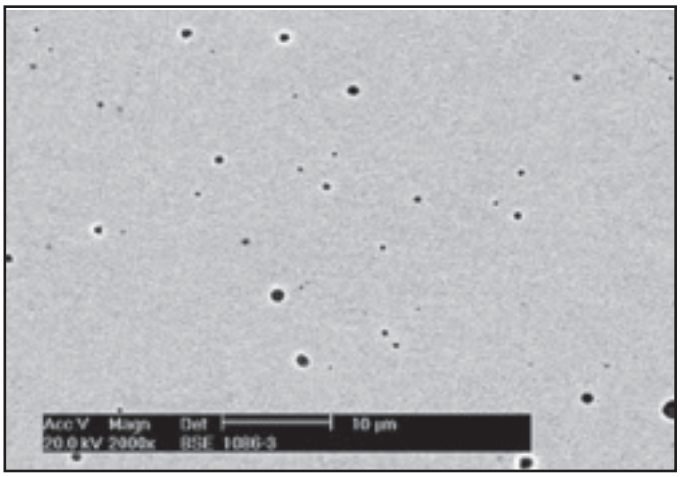

Fig. 2 — Backscattered electron image from a sample in the polished condition.

listed in Table 1. In most of the cases, the thickness of the base material was about 20 mm (0.75 in.). The base materials were cut into 152- × 711-mm (6- × 28-in.) sections to accommodate the various test welds and experimental specimens. The base materials were joined by the welding processes described below. Figure 1 shows a general view of a welded joint prepared for weld metal characterization in this study.

Welding Procedures and Consumables

In an attempt to cover a broad range of applications normally found in different industries, different welding processes and commercially available consumables were used in this program. Welds were produced using flux-shielded processes such as flux cored arc welding (FCAW) and shielded metal arc welding (SMAW) and gas-shielded processes such as gas metal arc welding (GMAW). FCA welding included both self- (T-8 Type) and gas-shielded electrodes. Cellulosic and basic electrodes were used with the SMAW process. The nominal strength of the weld deposits ranged from 490 to 840 MPa (70 to 120 ksi). Table 1 provides a summary of the consumables, welding processes, and weld identifications (W1 to W14) used in this study. Welding parameters are summarized in Table 2.

Weld Metal Chemical Analysis

Samples for chemical analysis were taken from the reduced area of tensile specimens. Chemical analysis of the experimental welds was conducted using an optical emission spectrometer. LECO equipment was used to measure carbon, sulfur, oxygen, and nitrogen.

Weld Metal Microstructural Characterization

Microstructural analysis was conducted using light microscopy, conventional scanning electron microscopy (SEM), and high-resolution SEM. Due to the important role played by the inclusions on the microstructure development and the resulting mechanical properties of the steel weld deposits, particular attention was given to the inclusion characteristics, including volume fraction, size distribution, morphology, and chemical composition. Carbon replica extraction techniques were used for the chemical composition and morphology analysis of the inclusions.

Cross sections were cut from each weld and prepared using standard metallo-

Table 1 — Summary of Base Metals, Welding Processes, Welding Consumables, and Identification of Different Weld Metals Characterized in This Program

Welded Joint	Base Metal	Welding Process	Welding Condition	Filler Metal	Procedure/Shielding Gas
W1	Plate, SA-36	FCAW	Semiautomatic	E71T-1[a]	CO_2
W2	Plate, SA-36	FCAW	Semiautomatic	E71T-1	CO_2
W3	Unknown	GMAW	Semiautomatic	ER70S-7[b]	CO_2
W4	Unknown	GMAW	Semiautomatic	ER70S-6[c]	CO_2
W5	Pipe, X80	SMAW	Manual	E8010-G	NA
W6	Pipe, X80	SMAW	Manual	E9010-G	NA
W7	Pipe, X80	SMAW	Manual	E9018-G	NA
W8	Pipe, X80	FCAW-S	Semiautomatic	E91T8-G	NA
W9	Plate, X100	GMAW	Automatic	ER100S-1[b]	Internal/external 100 CO_2
W10	Plate, X100	GMAW	Automatic	ER100S-1[c]	Internal/external, pulsed, 85 Ar-15 CO_2
W11	Plate, X100	GMAW	Automatic	ER100S-1[c]	Internal/external, dual torch, pulsed, 85 Ar-15 CO_2
W12	Plate, X100	GMAW	Automatic	ER100S-1[b]	External, pulsed, 95 Ar-5 CO_2
W13	Plate, X100	GMAW	Automatic	ER120S-1	Internal-external 100 CO_2
W14	Plate, X100	GMAW	Automatic	ER120S-1	Internal/external, pulsed, 85 Ar-15 CO_2

(a) Microalloyed; (b) and (c) represent different wire manufacturer.

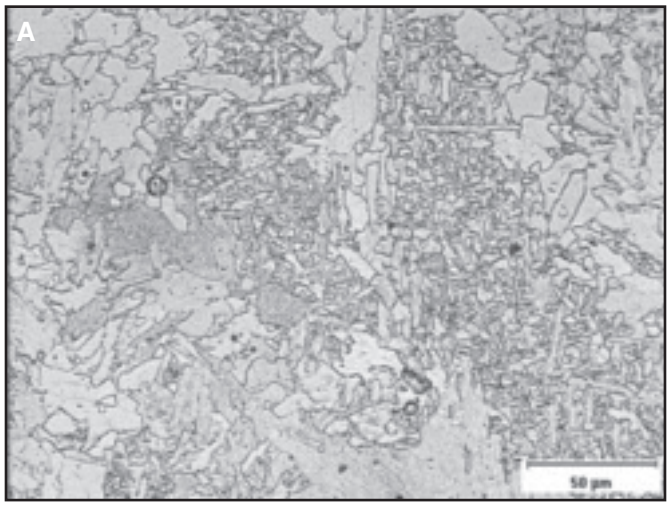

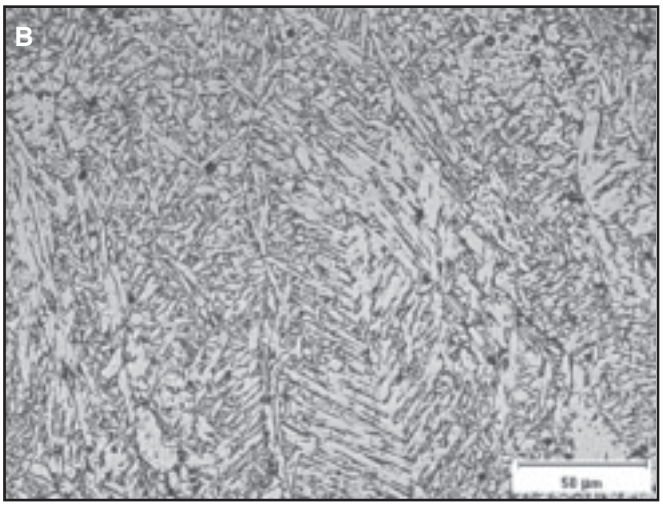

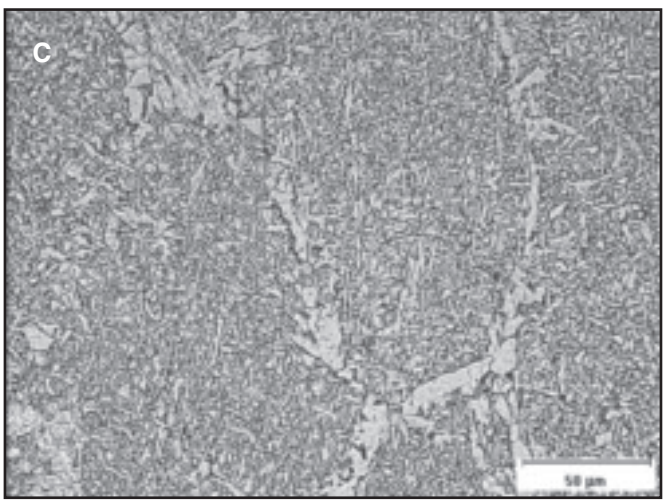

Fig. 3 — Microstructural characteristics of primary weld region. A — Weld metal W2 (CE_{IIW} = 0.257); B — weld metal W6 (CE_{IIW} = 0.31); and C — weld metal W7 (CE_{IIW} = 0.39).

graphic techniques. For replica extraction, samples were prepared by grinding through 800-grit abrasive paper and then polishing using 6-, 3-, and 1-µm diamond paste. Final polishing of samples for light microscopy and SEM samples was done with 1- and 0.05-µm chromium oxide slurry. In this way, alumina contamination of the samples was avoided.

The weld metal microstructure was revealed by etching in a 2% Nital solution. Etching for replica extraction was done with a 5% Nital reagent. A light etching was used in order to expose the inclusions on the surface and permit their extraction. In order to avoid inclusion dissolution or damage during polishing and prior to replica extraction, ethyl alcohol was used at all times for diamond paste dispersion and sample cleaning. For the same reason, long ultrasonic cleaning times were avoided.

The samples prepared for inclusion size and size distribution measurements on the SEM were in the as-polished (unetched) condition. A minimum of 20 backscattered electron images from the as-polished samples, similar to the one shown in Fig. 2, were recorded on the SEM and analyzed to measure the inclusion size distribution. The backscattering electron images were obtained from the central region of the weld fusion zone at random locations in the through-thickness direction. SEM analysis was performed on a high-resolution field emission microscope coupled with XEDS for chemical analysis. The image analysis of the SEM images was performed with *Image-Pro* software.

Results and Discussions

Chemical Composition Analysis

The chemical compositions of the weld metals deposited with electrodes of E70X-E80X (W1 to W5), E90X (W6 to W8), and E100X-E120X (W9 to W14 nominal tensile strength are listed in Tables 3, 4, and 5, respectively. In general, the deposited HSS weld metals are based on a C-Mn system with additions of deoxidizers (silicon, manganese, aluminum, titanium) and balanced additions of various alloying elements (nickel, chromium, molybdenum, boron, niobium, vanadium, copper).

The chemical composition of weld metals is controlled by chemical reactions occurring in the weld pool at elevated temperatures, and is therefore influenced by the welding consumables (i.e., combination of filler metal, flux, and/or shielding gas), the base metal chemistry, as well as the welding conditions applied. Even small changes in the flux coating can result in large variations in the metallurgical behavior of the flux system (Ref. 6).

As expected, the level of alloying content in the weld metal increases as the nominal strength of the consumables increases. Alloying elements strengthen the weld metal through solid solution or precipitation strengthening. Alloying elements also affect the hardenability of the weld metal and play a significant role in defining the final weld metal microstructure. The effect of alloying levels on the hardenability of the weld metal is reflected in the carbon-equivalent numbers (CE_{IIW} and Pcm). The carbon equivalent of weld metals deposited with E70X-E80X, E90X, and E100X–E120X grade consumables range from 0.25 to 0.35, 0.31 to 0.54, and 0.47 to 0.73, respectively, as listed in Tables 3–5.

The carbon content of most of the deposited weld metals ranged from 0.05 to 0.1%. There were major differences in carbon content ranges among welds deposited with different welding processes or groups of welding consumables.

The welding process selected to join HSSs greatly influences the level of oxygen and nitrogen in the weld metals. Table 6 shows a summary of the different levels of oxygen and nitrogen observed in the weld metals deposited with different welding processes and consumables.

Partial oxidation almost invariably accompanies the welding of steel due to reactions of the molten metal with the shielding gas or flux (Ref. 7). The solubility of oxygen in pure liquid iron is approximately 1600 parts per million (ppm) at the melting point (Ref. 8). During solidification, this

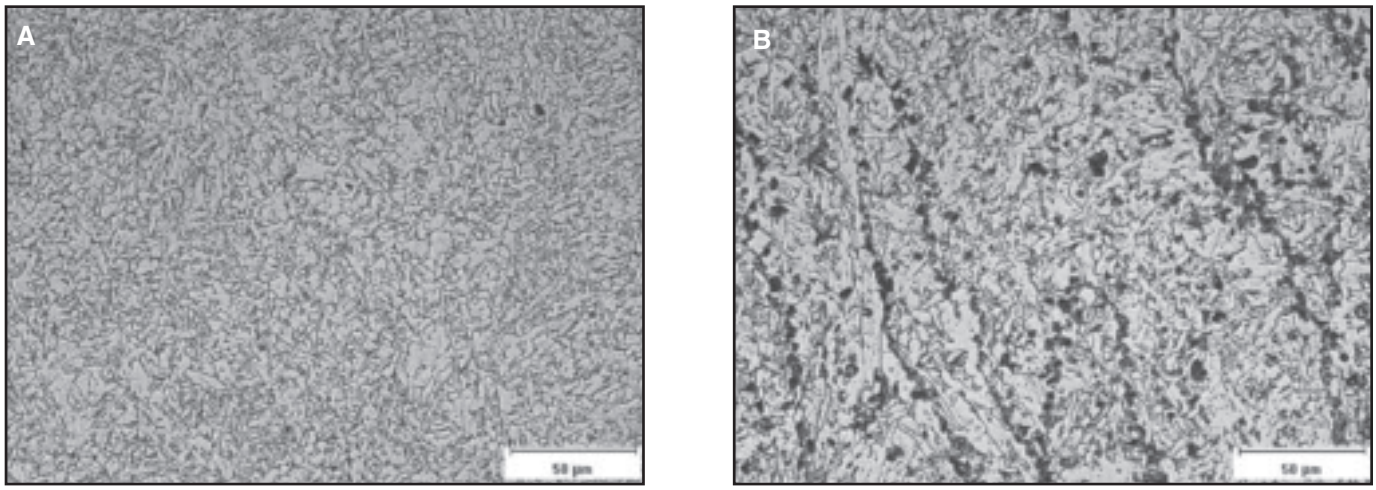

Fig. 4 — Microstructural characteristics of reheated weld region. A — Weld metal W7 (CE_{IIW} = 0.39); B — weld metal W6 (CE_{IIW} = 0.31).

decreases to about 860 ppm at 1500°C in delta iron. Most of the alloying elements present in liquid steel reduce oxygen solubility through deoxidation equilibrium. Steelmaking processes typically yield analytical oxygen levels in the range of 70 to 100 ppm. Welds typically pick up oxygen to levels of several hundred ppm, then deoxidize to lower oxygen levels with the formation of oxide inclusions.

The oxygen levels of weld metals are influenced by many factors such as the amount of deoxidizers present (silicon, manganese, aluminum, etc.), the types of welding materials used, the welding process (Refs. 9, 10), and the welding conditions. Weld metal deposited with flux-shielded processes or with active gas-shielded processes generally contains more oxygen than welds deposited with inert gas-shielded processes. The oxygen levels of weld metals deposited with SMAW, FCAW (gas shielded), and GMAW with 100% CO_2 ranged from 450 to 650 ppm. On the other hand, welding with the GMA process shielded with Ar-CO_2 mixtures resulted in an oxygen content range of 260 to 360 ppm in the weld metals. The oxygen level of weld metals deposited with self-shielded FCAW was 110 ppm.

Flux-shielded metal arc weld metals generally contain more nitrogen than those made with gas-shielded welding processes. The nitrogen content in weld metals deposited with flux-shielded processes ranged from 70 to 370 ppm. The weld metal with the highest nitrogen content corresponds to that deposited with the self-shielded flux-cored wire. Weld metals deposited with the GMAW process contained nitrogen levels from 30 to 140 ppm. In general, a consumable/process could be classified as low, medium, or high nitrogen if the amount of nitrogen in the metal weld deposit is less than 70 ppm, between 70 to 120 ppm, or greater than 120 ppm, respectively (Refs. 11, 12).

Table 2 — General Welding Conditions Used to Deposit Weld Metals W1 to W14

Welded Joint	Welding Consumable		Preheat/Interpass	Nominal Heat
	Root Pass	Fill Pass	Temperature, °C	Input, kJ/mm
W1	E71T-1[a]	E71T-1[a]	RT/150	1.8 to 2.0
W2	E71T-1	E71T-1	RT/150	1.8 to 2.0
W3	ER70S-7	ER70S-7	Unknown	Unknown
W4	ER70S-6	ER70S-6	Unknown	Unknown
W5	E8010-G	E8010-G	RT/120	1.3
W6	E9010-G	E9010-G	RT/120	1.5
W7	ER70S-6, STT[b]	E9018-G	RT/120	1.3
W8A[c]	ER70S-6, STT[b]	E91T8-G	RT/110	0.9
W8B[d]	ER70S-6, STT[b]	E91T8-G	RT/120	1.2
W8C[e]	ER70S-6, STT[b]	E91T8-G	RT/52	1.1
W8D[f]	ER70S-6, STT[b]	E91T8-G	RT/290	1.0
W9	ER100S-1	ER100S-1	50/150	0.76
W10	ER100S-1	ER100S-1	50/150	0.80
W11	ER100S-1	ER100S-1	50/150	0.9
W12	ER100S-1	ER100S-1	50/150	0.82
W13	ER120S-1	ER120S-1	50/150	0.77
W14	ER120S-1	ER120S-1	50/150	0.85

(a) Microalloyed; (b) surface tension transfer®; (c) welder A; (d) welder B; (e) low interpass temperature (cold); (f) high interpass temperature (hot).

Microstructure Characterization

In general, two major trends were observed in the change of the microstructure of the weld metal as the carbon equivalent increased. The fraction of low-temperature products increased and the microstructure became finer as the carbon equivalent increased.

Lean steel weld metals exhibit low hardenability, and the hardenability increases with alloy content. Weld metals lean in alloy content would be expected to transform at relatively high temperatures to produce a microstructure often consisting of ferrite and carbides having low strength. An increase in the amount of alloying elements, particularly the carbide formers, lower the transformation temperature, and form a bainitic structure having a smaller mean free-path in the ferrite. As additional quantities of alloying elements are introduced, further lowering of the transformation temperature occurs, producing a finer bainitic structure and a stronger weld metal. Finally, if the alloy content is increased to a point where martensite forms, the strength reaches a level primarily dictated by the carbon content in the weld metal.

The as-deposited weld metals with a carbon equivalent between 0.26 (W2) and 0.39 (W7) consist mainly of a ferritic microstructure with a decreasing fraction of grain boundary ferrite and an increasing fraction of lower temperature transforma-

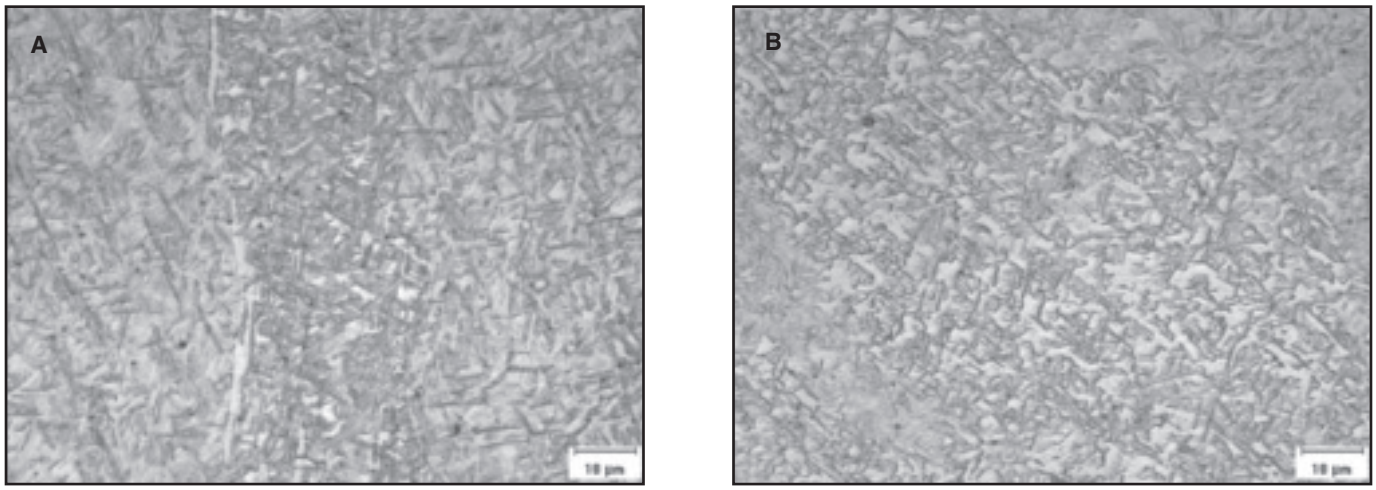

Fig. 5 — Microstructural characteristics. A — Primary weld region; B — reheated weld region of weld metal W14 (CE_{IIW} = 0.73).

tion products such as sideplate ferrite and acicular ferrite. In the microstructure of weld metal W2 a high fraction of grain boundary ferrite was present, as shown in Fig. 3A. Increasing the carbon equivalent to 0.31 (W6) resulted in a microstructure consisting predominantly of sideplate ferrite with aligned second phases as shown in Fig. 3B. In the microstructure of the as-deposited weld metal W7 (CE_{IIW} = 0.39) a high fraction of acicular ferrite is present, as shown in Fig. 3C.

In general, the reheated region of these welds transformed to equiaxed polygonal ferrite as shown in Fig. 4. In the reheated zones of weld metal W5 and W6, a high fraction of second-phase precipitates that could be pearlite and/or carbide aggregates was present. This observation may be explained based on the high level of carbon present in these weld metals and on the segregation of carbon out of the ferrite grain during the retransformation induced during cooling of the weld metal. The carbon content of weld metal W5 and W6 was 0.1 and 0.15%, respectively. These observations clearly indicate that the influence of thermal cycles resulting from subsequent passes can cause significant changes in weld metal microstructure and resulting properties.

Acicular ferrite is the weld metal constituent that has been reported to best promote toughness in HSLA steels with around 600-MPa (85-ksi) yield strength or less because of its small grain size (typically 1 to 3 μm) and because of the random orientation of the ferrite laths and their ability to deflect cracks during propagation (Ref. 13). As such, a large amount of acicular ferrite optimizes the weld metal mechanical properties.

Hardenability of these steel weld metals is such that welds with a mainly bainitic and/or martensitic microstructure usually can be avoided, and the major problem becomes one of preventing the formation of grain boundary ferrite, while refining the acicular ferrite as much as possible.

Factors that affect the amount of grain boundary ferrite, such as specific microalloying additions like boron and titanium and the prior austenite grain size are important considerations (Ref. 14). Likewise, factors that directly affect the acicular ferrite transformation such as inclusion composition, inclusion size, and crystallographic or thermal disregistry between the inclusion and the austenite matrix become of crucial concern. The literature is not in agreement on the effect of specific types of inclusions on the austenite to ferrite phase transformation. However, the effectiveness of an inclusion in nucleating ferrite may not depend on its bulk composition, but on its surface composition and character (Ref. 15).

In weld metals with a carbon equivalent of 0.47 or higher (W8 to W14), an increasing fraction of lower transformation products, including martensite, were observed as shown in Fig. 5A. Additionally, it was observed that weld metals with higher alloying additions do not readily retransform during reheating induced during multipass welding. As shown in Fig. 5B, the microstructure

Table 3 — All Weld Metal Chemical Composition (wt-%) of E7X-E8X Weld Metals

Element	Welded Joint				
	W1 E71T-1[a]	W2 E71T-1	W3 ER70S-7	W4 ER70S-6	W5 E8010-G
C	0.054	0.021	0.066	0.056	0.1
Mn	1.35	1.31	1.41	1.35	0.66
P	0.009	0.008	0.012	0.011	0.009
S	0.009	0.012	0.005	0.004	0.005
Si	0.42	0.40	0.36	0.5	0.12
Cu	0.07	0.05	0.22	0.18	<0.01
Ni	0.40	0.01	0.06	0.04	0.71
Cr	0.05	0.04	0.04	0.05	0.02
Mo	0.01	0.01	0.12	0.06	<0.01
Al	<0.01	<0.01	0.01	0.01	<0.01
V	0.02	0.02	0.005	<0.005	0.02
Ti	0.04	0.03	0.02	0.02	0.006
Nb	0.010	0.010	0.03	0.02	<0.005
O	0.0520	—	0.046	0.046	0.065
N	0.0073	—	0.003	0.008	0.021
B	0.0053	0.0048	<0.0005	<0.0005	<0.0005
Zr	<0.005	<0.005	<0.005	<0.005	<0.005
W	<0.01	<0.01	<0.02	<0.02	<0.01
$CE_{(IIW)}$	0.326	0.257	0.353	0.319	0.268
Pcm	0.177	0.131	0.172	0.157	0.151

(a) Microalloyed.

Table 4 — All Weld Metal Chemical Composition (wt-%) of E9X Weld Metals

Element	Welded Joint W6 E9010-G	W7 E9018-G	W8A E91T8-G	W8C E91T8-G	W8D E91T8-G
C	0.154	0.06	0.071	0.084	0.074
Mn	0.73	1.55	2.07	2.30	2.18
P	0.017	0.017	0.010	0.009	0.006
S	0.013	0.006	0.007	0.008	0.007
Si	0.17	0.47	0.25	0.29	0.29
Cu	0.023	0.126	0.06	0.043	0.062
Ni	0.69	0.72	0.69	0.86	0.75
Cr	0.06	0.06	0.02	0.03	0.03
Mo	0.06	0.02	0.06	0.02	0.06
Al	<0.01	0.01	0.78	1.02	0.81
V	—	—	—	—	—
Ti	<0.012	0.008	0.006	0.006	0.005
Nb	—	—	—	—	—
O	0.050	0.046	0.011	0.011	0.011
N	0.011	0.012	0.037	0.0323	0.0323
B	—	—	—	—	—
Zr	0.002	<0.001	0.072	0.11	0.075
W	—	—	—	—	—
$CE_{(IIW)}$	0.310	0.390	0.482	0.537	0.509
Pcm	0.220	0.156	0.203	0.228	0.215

Table 5 — All Weld Metal Chemical Composition (wt-%) of ER100S-ER120S Weld Metals

Element	Welded Joint W9 ER100S-1	W10 ER100S-1	W11 ER100S-1	W12 ER100S-1	W13 ER120S-1	W14 ER120S-1
C	0.068	0.061	0.068	0.055	0.11	0.100
Mn	1.45	1.46	1.25	1.50	1.51	1.76
P	0.008	0.007	0.008	0.009	0.014	0.013
S	0.004	0.003	0.006	0.003	0.010	0.010
Si	0.250	0.250	0.250	0.370	0.59	0.56
Cu	0.100	0.070	0.090	0.120	0.11	0.12
Ni	1.43	1.74	1.64	1.75	1.82	2.29
Cr	0.08	0.09	0.09	0.040	0.34	0.41
Mo	0.33	0.33	0.31	0.420	0.45	0.44
Al	0.01	0.01	<0.010	0.020	0.01	<0.010
V	0.01	0.009	0.010	0.010	0.01	0.010
Ti	0.01	0.01	0.008	0.020	0.02	0.020
Nb	0.01	<0.005	0.007	0.010	0.008	0.006
O	0.056	0.031	0.036	0.026	0.045	0.028
N	0.007	0.008	0.014	0.004	0.006	0.009
B	<0.0005	<0.0005	<0.0005	<0.0005	<0.0005	<0.0005
Zr	—	—	—	—	—	—
W	—	—	—	—	—	—
$CE_{(IIW)}$	0.496	0.485	0.471	0.524	0.651	0.726
Pcm	0.204	0.202	0.197	0.208	0.289	0.302

of the reheated weld metal is very similar to the microstructure of the as-deposited weld metal. The kinetics of grain boundary mobility may be significantly retarded in highly alloyed weld metal by substitutional alloy elements. Additionally, the high hardenability of these weld metals decreases the role of grain boundaries as nucleation sites of phase transformation during cooling.

Therefore, although the carbon equivalents were originally developed with the goal of evaluating the base metal cold cracking susceptibility, these empirical equations can also be useful for clarifying the complex relationship between the weld metal content of hardenability elements and the resulting transformation behavior of the deposit. However, there is the need to modify the carbon-equivalent equations by including the role of weld metal oxygen and the influence of welding parameters such that they become more effective in predicting weld metal properties (Ref. 16). More recent efforts in heat-affected zone (HAZ) studies have developed weldability expressions that include cooling rate (Ref. 13).

Table 6 — Oxygen and Nitrogen Levels in Weld Metals Deposited with Different Welding Processes and Consumables

Process	Consumables	Oxygen (ppm)	Nitrogen (ppm)
FCAW	E70X, rutile, 100% CO_2	520	70
FCAW	E90X, self shielded	110	370
SMAW	E80X, cellustic	650	210
SMAW	E90X, cellustic	500	110
SMAW	E90X, basic	460	120
GMAW	E70X, 100% CO_2	460	30–80
GMAW	E100X, 100% CO_2	560	70
GMAW	E120X, 100% CO_2	450	60
P-GMAW	E100X, 85Ar-15CO_2	310 to 360	80 to 140
P-GMAW	E120X, 85Ar-15CO_2	280	90
P-GMAW	E100X, 95Ar-5CO_2	260	40

Nonmetallic Inclusion Characterization

Quantitative data obtained from measurements of inclusions in different weld metals, including average inclusion size, maximum inclusion size, inclusion density, and volume fraction are listed in Table 7.

Volume Fraction and Inclusion Density

The volume fraction of nonmetallic inclusions in most deposited weld metals ranged from 0.2 to 0.6%. In a few welds, however, the volume fraction of the nonmetallic inclusions was as high as 0.8 to 1.1%.

Different researchers have suggested that weld inclusion contents (vol-%) may be estimated from an empirical relation involving both oxygen and sulfur concentrations (Refs. 17, 18). Additionally, it has been observed that the manganese/silicon ratio of a weld is important in controlling inclusion contents (Refs. 19, 20). The actual levels of manganese and silicon can affect the inclusion volume fraction because of their influence on the melting range of the inclusions and the ease with which inclusions are removed from liquid metal into the welding slag.

Figure 6 shows the volume fraction of nonmetallic inclusions as a function of the oxygen plus sulfur content in the weld

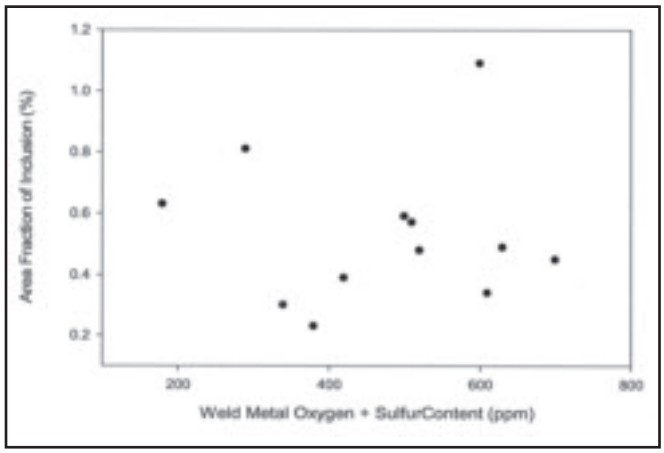

Fig. 6 — Volume fraction of inclusions as function of oxygen + sulfur content in the deposited weld metals.

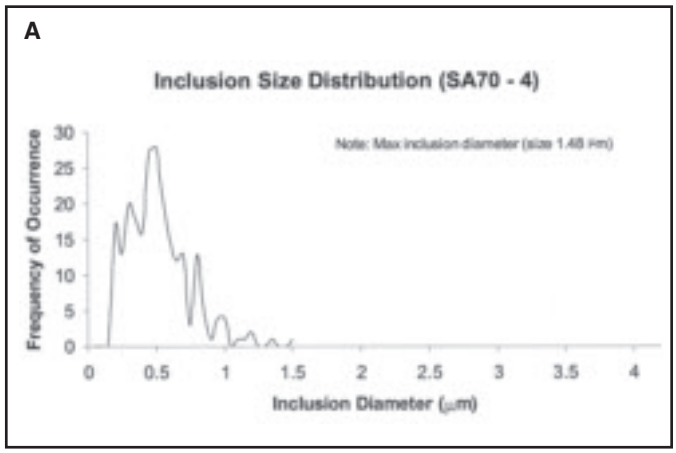

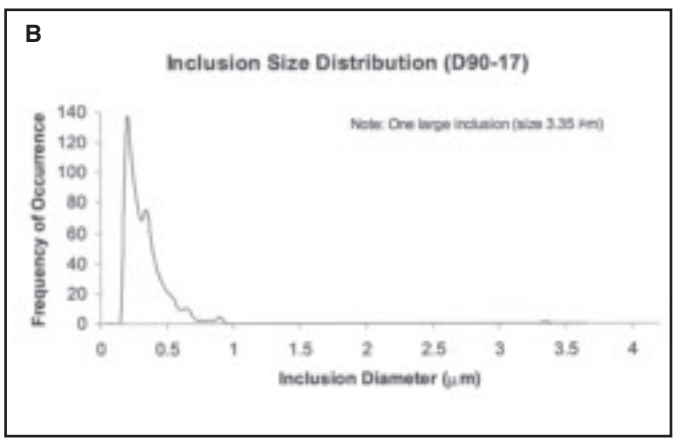

Fig. 7 — Measured inclusion histogram. A — Weld metal W5; B — weld metal W7.

metals. In general, the volume fraction of inclusions increases with an increase in oxygen plus sulfur content in the weld metal. However, the opposite trend was observed in the volume of nonmetallic inclusions with sulfur plus oxygen levels higher than 500 to 600 ppm. The inclusion density does not show a clear trend with oxygen plus sulfur levels in the weld metal of up to 550 ppm. However, the inclusion density decreases with increasing oxygen plus sulfur levels above 550 to 600 ppm. The inclusion density observed in the welds ranges from 1.2×10^8 to 5.4×10^8 particles per mm^3.

Size Distribution

From the data listed in Table 7, it may be seen that the average inclusion diameter ranged from 0.3 to 0.6 μm and maximum inclusion diameter from 0.9 to 1.7 μm in the deposited weld metals. Examples of measured inclusion histograms are presented in Fig. 7A and 7B. The histograms shown in Fig. 7A and 7B correspond to the nonmetallic inclusion population observed in welds W5 and W7, respectively. In weld W5, the average inclusion size, the maximum inclusion size, and the inclusion density were 0.491 μm, 1.48 μm, and 1.94×10^8 particles/mm^3, respectively. On the other hand, in weld W7, an average inclusion diameter, a maximum inclusion diameter, and an inclusion density equal to 0.31 μm, 0.95 μm, and 4.55×10^8 particles per mm^3, respectively, were observed.

As can be observed in Fig. 7, some histograms showed the presence of a sparse population of inclusions, which are coarser than that indicated by the tail of the upper end of the size distribution. The maximum size of this group of inclusions in the different weld metals ranged from 1.6 to 3.4 μm.

In welds deposited with SMAW, the particle size distribution was observed to be dependent on the flux basicity. Welds produced with cellulosic electrodes (W5 and W6) showed larger average inclusion size, larger maximum inclusion size, and lower inclusion population than welds produced with basic electrodes (W7). This finding is not surprising considering the high oxygen potential and low desulfurization capacity of slags formed by cellulosic electrodes. However, the volume fraction of inclusions is of the same order of magnitude in both cases (0.45 and 0.48%), indicating that the higher oxygen and sulfur concentrations of the weld deposited with cellulosic electrodes are mainly a result of a different inclusion size distribution as compared to basic welds.

A similar trend was observed in the size distribution of inclusions observed in weld metal deposited with gas-shielded FCAW electrodes (W1 and W2) compared to the weld deposited with self-shielded FCAW electrodes (W8). The narrower and finer size distribution of inclusions observed in FCAW-S welds compared to gas-shielded FCAW welds could be explained based on the lower oxygen plus sulfur concentration in the weld metal. The oxygen plus sulfur concentrations in welds W1 and W8 were 610 and 180 ppm, respectively.

Figure 8A and 8B show the average and maximum inclusion size as a function of oxygen plus sulfur content in the weld metal. As observed in Fig. 8A, the average inclusion size does not drastically change with oxygen plus sulfur levels up to about 400 ppm. However, above 400 ppm, the average inclusion size increases with an increase in oxygen plus sulfur level in the weld metal. On the other hand, the maximum inclusion size, as indicated by the tail of the upper end of the size distribution, is not greatly dependent on the level of oxygen and sulfur in the weld metal, as shown in Fig. 8B.

Additionally, the maximum size of the scarce population of inclusions, which are coarser than the size indicated by the upper end of the size distribution, seems to reach a plateau of about 3.2 μm at oxygen plus sulfur levels between 300 and 600 ppm. This observation may be explained based on the increasing ability of an inclusion to float to the surface of the weld pool as its size increases. From deoxidation of liquid steel, it is well established that the flotation rate of the oxides generally depends on their growth rates, since large inclusions separate much more rapidly than small ones, in agreement with Stokes' law (Ref. 7).

The ability of inclusions to float to the surface of the weld pool as a function of their size also helps to explain the decrease in volume fraction and inclusion density of nonmetallic inclusions observed

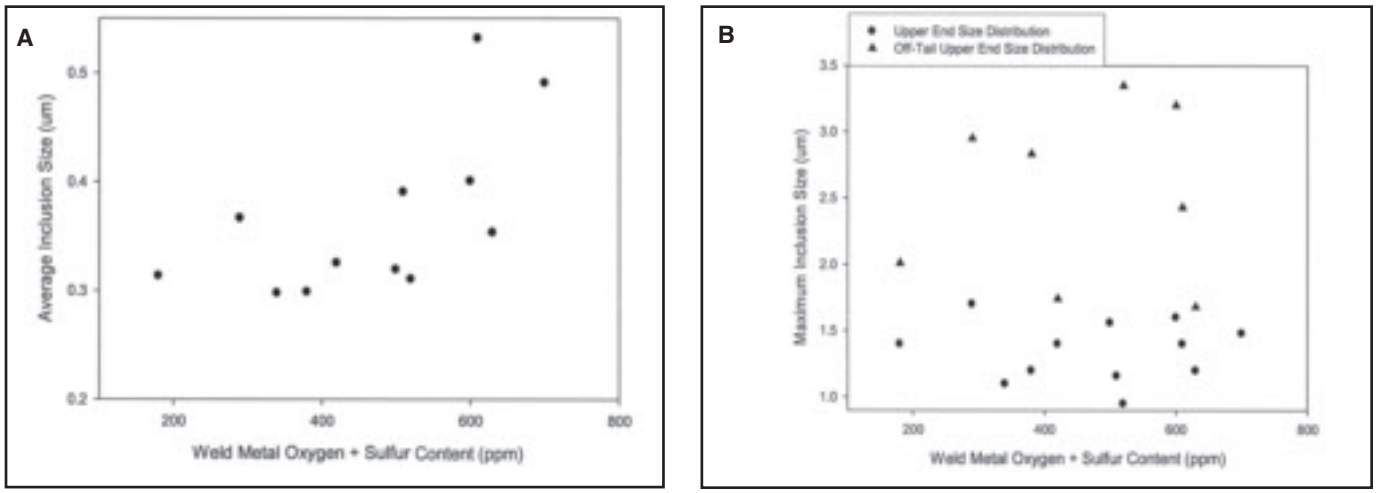

Fig. 8 — A — Average inclusion size; B — maximum inclusion size as function of oxygen + sulfur content in the weld metal.

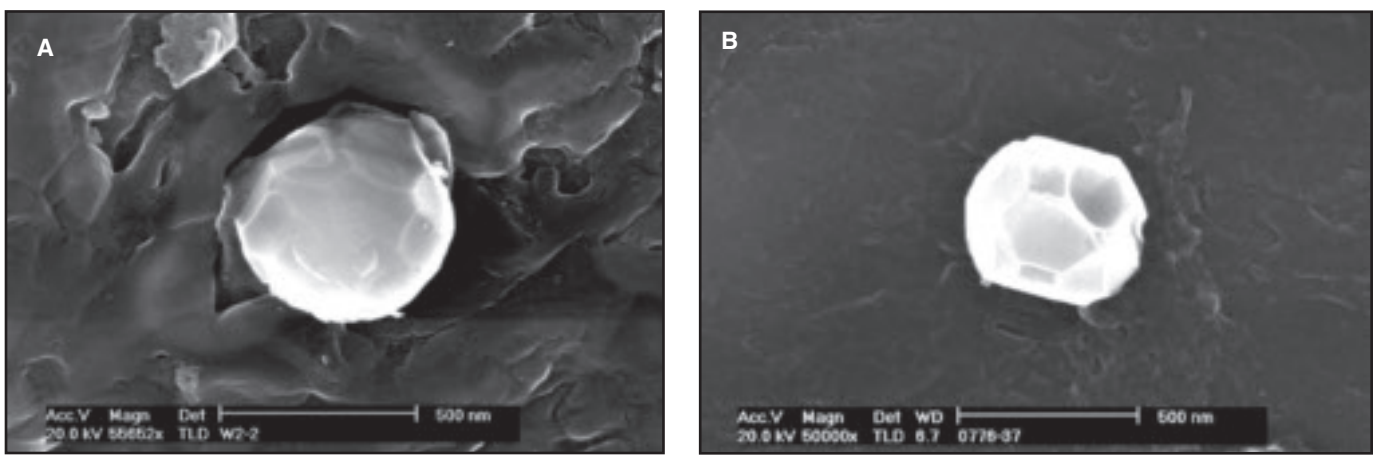

Fig. 9 — Image of inclusion observed. A — Weld metal W9; B — in weld metal W4.

Table 7 — General Characteristics of Nonmetallic Inclusions Observed in Weld Metals W1 to W14

Specimen	Average Inclusion Diameter (μm)	Maximum Inclusion Size (μm)	Number of Inclusions per mm^3 ($\times 10^8$)	Volumetric Fraction of Inclusion (%)
W1	0.532	1.4 (2.43)[a]	1.21	0.34
W2	0.517	1.6 (2.43)[a]	1.36	0.4
W3	0.391	1.16	4.0	0.57
W4	0.32	1.56	5.39	0.59
W5	0.491	1.48	1.94	0.45
W6	0.354	1.2 (1.68)[a]	3.68	0.49
W7	0.311	0.95 (3.35)[a]	4.55	0.48
W8	0.314	1.4 (2.01)[a]	5.39	0.63
W9	0.401	1.6 (3.2)[a]	4.64	1.09
W10	0.298	1.1	3.53	0.3
W11	0.326	1.4 (1.74)[a]	3.54	0.39
W12	0.367	1.7 (2.95)[a]	4.22	0.81
W13	NA	NA	NA	NA
W14	0.299	1.2 (2.83)[a]	2.17	0.23

(a) Represent an observed maximum inclusion size; however, this size was much bigger than the end of the upper tail of the size distribution observed in the particular weld.

with increasing oxygen plus sulfur levels above 500 ppm. As the average inclusion size increases, the probability of more inclusions to float to the surface of the weld pool increases and, as a result, the volume fraction and inclusion density of nonmetallic inclusions may decrease.

Shape and Composition of Weld Metal Inclusions

Nonmetallic inclusions are almost always heterogeneous in nature both with respect to shape (angular or spherical particles) and chemistry (multiphase particles) as a result of the complex alloying systems involved.

Figures 9 and 10 show examples of inclusions of different shapes and textures observed in the weld metals. The observed inclusions present shapes that include spherical, faceted, and agglomerations of particles. The chemical compositions of some of the inclusions observed in differ-

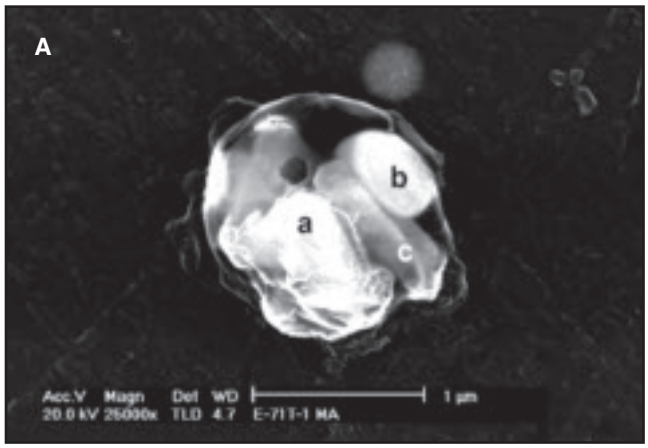

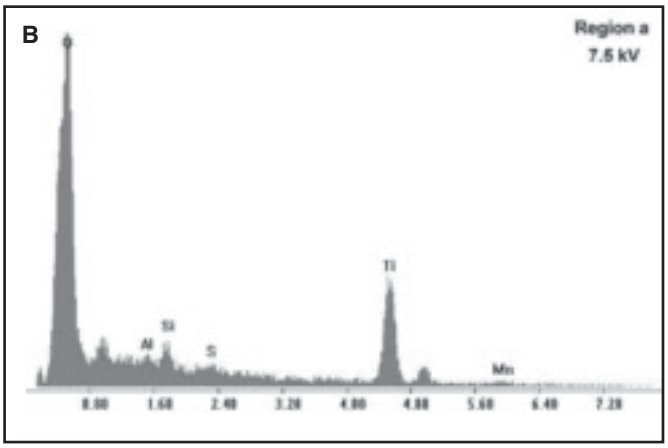

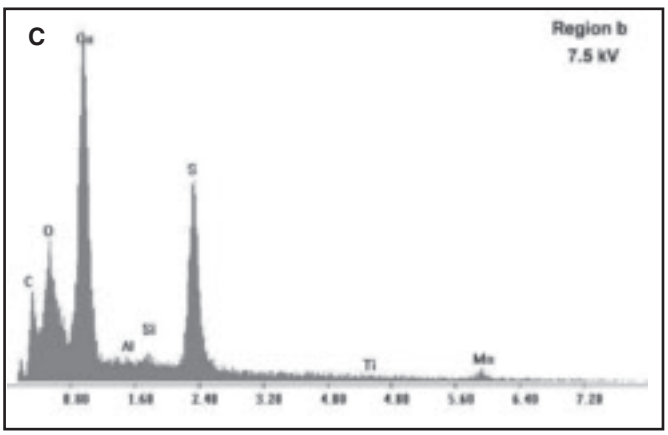

Fig. 10 — A — Image; B and C — associated EDX-spectra of inclusion observed in weld metal W1. [Description: composite inclusion; chemical composition: region A 32.2O-0.5Al-1.3Si-0.9S-51.4Ti-13.7Mn (Ti-O_2), region B MnS, region C Ti-oxide.]

ent weld metals are listed in Table 8. Generally, the inclusion core consists mainly of a mixture of oxides of titanium, manganese, silicon, and aluminum in different proportions, reflecting a very complex deoxidation product. Conditions in the molten pool approach equilibrium and, therefore, the stronger deoxidants such as titanium and aluminum occur in higher proportions in the inclusions than in the weld as a whole. Additionally, phases rich either in manganese and sulfur; silicon; or zirconium, carbon, and nitrogen, which indicates the presence of manganese sulfides, silica, or zirconium carbonitrides were also observed.

Figure 10B and C shows some of the spectra obtained from the analysis of the inclusions by EDX-microprobe analysis. Most of the carbon in the spectrum is due to the carbon film that supports the inclusions. The copper and zinc in the spectra are due to the sample holder used.

Analysis by EDX-microprobe analysis also confirmed the existence of several phases within inclusion agglomerates. Figure 10B and C show the spectra obtained from the different areas of the inclusion agglomerate shown in Fig. 10A. Region A corresponds to an oxide rich in titanium and manganese with a small proportion of aluminum and silicon; region B seems to correspond to a manganese sulfide; and region C is mainly a titanium oxide.

A sequence of inclusion formation in Al-Ti-Si-Mn deoxidized steel weld metals has been proposed by some researchers and outlined as follows (Ref. 7). In general, the inclusions consist of an oxide core, which is formed during the primary deoxidation stage. The chemical composition of the deoxidation products can vary within wide limits, depending on the relative activities of aluminum, titanium, silicon, manganese, and oxygen in the weld metal. The surface of the oxides will be covered partially by MnS and TiN. Precipitation of these phases occurs after the completion of the weld metal deoxidation, probably during solidification, where the reactions are favored by solute enrichment in the interdendritic liquid.

Conclusions

Based on the results and analysis of the experimental characterization of high-strength weld metal conducted during this study, the following conclusions are provided.

Chemical Composition

• The carbon equivalent (CE_{IIW}) of weld metal deposited with E70X–E80X, E90X, and E100X–E120X grade consumables ranges from 0.25 to 0.35, 0.31 to 0.54, and 0.47 to 0.73, respectively.

• The carbon content of most of the deposited weld metals ranges from 0.05 to 0.1%.

• The oxygen levels of weld metals deposited with SMAW, FCAW (gas shielded), and GMAW with 100% CO_2 ranges from 450 to 650 ppm. On the other hand, welding with the GMA process shielded with Ar-CO_2 mixtures resulted in an oxygen content range of 260 to 360 ppm in the weld metals. The oxygen level of weld metals deposited with self-shielded FCAW was 110 ppm. The nitrogen content in weld metals deposited with flux-shielded processes ranges from 110 to 370 ppm. Weld metals deposited with the GMAW process contained nitrogen levels from 30 to 140 ppm.

Microstructure

• The as-deposited weld metals with a carbon equivalent between 0.26 and 0.39 consist mainly of a ferritic microstructure with a decreasing fraction of grain boundary ferrite and an increasing fraction of sideplate ferrite and acicular ferrite. In general, the reheated region of these welds has transformed to equiaxed polygonal ferrite. The reheated zones of weld metal with carbon content between 0.1 and 0.15% present a high fraction of second phase precipitates that could be pearlite and/or carbide aggregates.

• In weld metals with a carbon equivalent of 0.47 or higher, an increasing fraction of lower temperature transformation products including martensite was observed. Additionally, it was observed that weld metals with higher alloying additions do not readily retransform during reheating induced during multipass welding.

Nonmetallic Inclusions

• The volume fraction of nonmetallic inclusions in most deposited HSS weld metals ranged from 0.2 to 0.6%. In a few welds, however, the volume fraction of nonmetallic inclusions was as high as 0.8

Table 8 — Characteristics of Nonmetallic Inclusions Observed in Different Weld Metals

Weld ID	Inclusion	Inclusion Characteristics: Chemical Composition	Inclusion Characteristics: Description
W1	1	Region A — 50.1O-0.7Mg-1.6Al-3.9Si-2.8S-19.6Ti-21.4Mn Region B — 48.2O-0.9Mg-1.6Al-3.4Si-2.3S-22.2Ti-21.4Mn	O, Al, Si, S, Ti, Mn rich
	2	51.4O-1.4Al-4.5Si-1.7S-18.1Ti-22.8Mn	O, Al, Si, S, Ti, Mn rich
	3	Region A — 32.2O-0.5Al-1.3Si-0.9S-51.4Ti-13.7Mn ($Ti-O_2$) Region b MnS, Region c Ti-Oxide	Composite inclusion
	4	Region A — 32.3O-1.5Al-0.7Si-50.4Ti-15.1Mn Region B — 35.4O-3.2Al-6.1Si-0.8S-26.5Ti-28.0Mn Region C — 35.3O-4.4Al-9.6Si-1.4S-3.6Ti-45.8Mn	Ti-Mn oxide
	5	30.9O-1.8Si-26.5S-3.5Ti-37.3Mn	Mn, S, O rich
	6	56.2O-1.3Al-5.5Si-2.1S-15.4Ti-19.5Mn	Ti-Mn oxide
	7	77.8O-0.9Si-1.3S-17.2Ti-2.8Mn	O, Si, S, Ti, Mn rich
W2	1	65.5O-0.5Si-1.4S-22.8Ti-9.8Mn	Ti oxide
	2	65.4O-2.5Si-13.0S-16.0Ti-3.1Mn	O, S, Ti rich
	4	67.9O-3.5Si-4.4S-21.1Ti-3.1Mn	Ti Oxide
	5	73O-1.9Al-6.9Si-1.0S-14.6Ti-2.7Mn	O, Al, Si, Ti, Mn rich
W3	1	55.1O-4.0Al-17.6Si-1.6S-3.6Ti-18.2Mn	O, Si, Mn rich
	2	55.9O-4.2Al-17.6Si-1.8S-2.4Ti-18.1 Mn	O, Al, Si, Mn rich
	3	Region A — 57.9O-4.6Al-17.4Si-1.9S-2.8Ti-15.5Mn Region B — 60.2O-1.7Al-2.2Si-0.6S-24.5-10.8	Composite inclusion
W4	1	33.7O-2.3Al-15.4Si-3.5S-6.5Ti-38.7Mn	O, Al, Si, S, Ti, Mn
	2	53.7O-5.0Al-17.6Si-2.0S-4.1Ti-17.6Mn	O, Al, Si, Ti, Mn rich
W5	1	68.6O-0.9Al-15.6Si-1.5S-2.9Ti-10.5Mn	O, Al, Si, S, Ti, Mn rich
	4	80.6O-0.7Al-14.0Si-2.1S-2.6Ti	O, Al, Si, S, Ti rich
W6	1	Region A — 49.9O-10.9Si-1.1S-12.0Ti-26.2Mn Region B — 49.3O-13.4Si-3.8S-3.9Ti-29.6Mn	O, Si, S, Ti, Mn rich
	2	12.1O-1.2Si-32.9S-53.8Mn	O, Si, S, Mn rich
	3	62.0O-9.8Si-0.7S-10.5Ti-17.0Mn	O, Si, S, Ti, Mn rich
	4	56.8O-1.9Al-16.0Si-2.1S-2.2Ti-21.1Mn	O, Al, Si, S, Ti, Mn rich
W8	1	47.0C-14.4N-10.9O-1.2Mg-2.0Al-24.5Zr	Zr Carbo-Nitride - Al_2O_3
	2	Region A — 23.0N-1.9Mn-7.9Al-66.6Zr-0.7Ti; Region B — 39.9N-23.4O-1.0Mg-30.3Al-5.4Zr	Composite inclusion
	3	45.4C-14.6N-15.6O-0.8Al-23.9Zr	Zr Carbo-Nitride
	4	40.3C-13.0N-13.4O-1.7Mg-2.8Al-28.7Zr	Zr Carbo-Nitride
	5	Region A — 40.4O-10.9Mg-23.0Al-25.7Zr Region B — 48.9O-15.0Mg-36.1Al	Composite inclusion
	6	Region A — 20.8N-33.2O-1.7Mg-1.6Al-42.7Zr Region B — 79.5O-20.5Zr	Composite inclusion
	7	Region A — 18.9N-29.2O-2.95Mg-3.0Al-46.0Zr Region B — 17.2N-40.8O-3.8Mg-13.9Al-24.3Zr	Composite inclusion
	8	11.2N-50.6O-14.2Mg-19.6Al-4.4Zr	Composite inclusion
	9-1	62.7O-3.4Mg-2.0Al-31.92Zr	O, Mg, Al, Zr rich
	10-2	56.0O-3.8Mg-29.5Al-10.8Zr	O, Al, Mg, Zr rich
	11-3	63.7O-36.3Si	SiO_2
W9	1	59.3O-13.2Al-9.0.Si-6.1Ti-12.4Mn	O, Al, Si, Ti, Mn rich
	2	65.0O-10.0Al-5.9Si-6.7Ti-12.5Mn	O, Al, Si, Ti, Mn rich
W10	1	59.5O-10.4Al-13.8Si-2.3Ti-14.0Mn	O, Al, Si, Ti, Mn rich
	2	63.7O-5.3Al-5.2Si-11.1Ti-14.7Mn	O, Al, Si, Ti, Mn rich

to 1.1%. The inclusion density observed in the welds ranged from 1.2×10^8 to 5.4×10^8 particles per mm^3. The average and maximum inclusion diameter ranged from 0.3 to 0.6 µm, and from 0.9 to 1.7 µm, respectively, in the deposited weld metals.

• In welds deposited with SMAW, the particle size distribution was observed to be dependent on the flux basicity. A similar trend was observed in weld metal deposited with gas-shielded FCAW electrodes as compared with welds deposited with self-shielded FCAW electrodes.

• The average inclusion size does not drastically change with oxygen plus sulfur levels up to about 400 ppm. However, above 400 ppm, the average inclusion size increases with an increase in oxygen plus sulfur level in the weld metal.

• Inclusions of different shapes and textures including spherical and faceted, and agglomerations of particles were observed in the weld metals. Generally, the inclusion core consists mainly of a mixture of oxides of titanium, manganese, silicon, and aluminum in different proportions, reflecting a very complex deoxidation product. Additionally, phases rich either in manganese and sulfur, silicon, or zirconium, carbon, and nitrogen, which indicates the presence of manganese sulfides, silica, or zirconium carbonitrides were also observed.

References

1. Denys, R. 1994. The properties of welded high strength steels. *Revue De La Soudure*, 26–39.

2. Dorling, D. V., Loyer, A., Russell, A. N., and Thompson, T. S. 1992. Gas metal arc welding used in mainline 80 ksi pipeline in Canada. *Welding Journal* 71(5): 55–61.

3. Chaudhari, V., Ritzmann, H. P., Wellnitz, G., Hillenbrand, H. G., and Willings, V. 1995. German gas pipeline first to use new generation line pipe. *Oil and Gas Journal*: 40–47, January 2.

4. Kawabata, F., Okatsu, M., Amano, K., and Nakano, Y. 1995. Metallurgical and mechanical features of X100 line pipe steel. *Pipeline Technology* Vol. 2: 263–271.

5. Hammond, J., and Millwood, N. A. 2000. Construction of ultrahigh-strength steel pipelines. In Pipeline Technology, *Proceedings, 3rd International Conference*, 69–88. Brugge, Belgium, May 21–24.

6. Liu, S., and Olson, D. L. 2003. Weld metal design:From flux coating to microstructure. *6th International Trends in Welding Research Conference Proceedings*, 529–535.

7. Kluken, A. O., and Grong, O. 1989. Mechanisms of inclusion formation in Al-Ti-Si-Mn deoxidized steel weld metals. *Metallurgical Transactions A* 20A(8): 1335–1349.

8. Frost, R. H., Olson, D. L., and Lu, S. 1993. Influence of solidification on inclusion formation in welds. *Proceedings 3rd International Conference on Trends in Welding Research*, 205–209.

9. Dorschu, K. E. 1977. Factors affecting weld metal properties in carbon and low alloy pressure vessel steels. *WRC 231*: 1–64.

10. Komizo, V., and Fukada, V. 1990. Toughness improvement in weld metal of carbon and HSLA steels in Japan. *First United States – Japan Symposium on Advances in Welding Metallurgy, Proceedings*, 358–381.

11. Wegrzyn, T. 2000. The classification of metal weld deposits in terms of the amount of nitrogen. *Proceedings, Tenth International Offshore and Polar Engineering Conference*, Vol. 4, 130–134.

12. Wegrzyn, T. 1996. Oxygen and nitrogen in SMAW and GMAW processes. *Proceedings, Sixth International Offshore and Polar Engineering Conference*, Vol. 4, 166–168.

13. Fleming, D. A., Bracarense, A. Q., Liu, S., and Olson, D. L. 1996. Toward developing a SMA welding electrode for HSLA-100 grade steel. *Welding Journal* 75(6): 171-s to 183-s.

14. Edwards, G. R., and Liu, S. 1990. Recent developments in HSLA steel welding. *First United States – Japan Symposium on Advances in Welding Metallurgy, Proceedings*, 213–292.

15. Ramsay, C. W., Matlock, D. K., and Olson, D. L. 1990. The influence of inclusions on the microstructures and properties of a high strength steel weld metal. *Proceedings, 2nd International Conference on Trends in Welding Research*, 763–767.

16. Ibarra, S., Olson, D. L., and Liu, S. 1991. Fundamental prediction of steel weld metal properties. *Journal of Offshore Mechanics and Artic Engineering* Vol. 113: 327–333, Nov.

17. Abson, D. J. 1989. Non-metallic inclusions in ferritic steel weld metals — a review. *Welding in the World* 27(3-4): 76–101.

18. Hong, T., and DebRoy, T. 1999. Oxide inclusions in the weld pool during submerged arc welding of low alloy steel. *Proceeding, 5th International Conference on Trends in Welding Research*, 185–190.

19. Dolby, R. E. 1976. Factors controlling weld toughness of weld metals. The Welding Institute, Report 14/1976.

20. Widgery, D. J. 1973. Deoxidation practice and toughness of mild steel weld metal. The Welding Institute, Report M/76/73.

Preparation of Manuscripts for Submission to the *Welding Journal* Research Supplement

All authors should address themselves to the following questions when writing papers for submission to the Welding Research Supplement:

- ◆ Why was the work done?
- ◆ What was done?
- ◆ What was found?
- ◆ What is the significance of your results?
- ◆ What are your most important conclusions?

With those questions in mind, most authors can logically organize their material along the following lines, using suitable headings and subheadings to divide the paper.

1) **Abstract.** A concise summary of the major elements of the presentation, not exceeding 200 words, to help the reader decide if the information is for him or her.

2) **Introduction.** A short statement giving relevant background, purpose, and scope to help orient the reader. Do not duplicate the abstract.

3) **Experimental Procedure, Materials, Equipment.**

4) **Results, Discussion.** The facts or data obtained and their evaluation.

5) **Conclusion.** An evaluation and interpretation of your results. Most often, this is what the readers remember.

6) **Acknowledgment, References and Appendix.**

Keep in mind that proper use of terms, abbreviations, and symbols are important considerations in processing a manuscript for publication. For welding terminology, the *Welding Journal* adheres to AWS A3.0:2001, *Standard Welding Terms and Definitions.*

Papers submitted for consideration in the Welding Research Supplement are required to undergo Peer Review before acceptance for publication. Submit an original and one copy (double-spaced, with 1-in. margins on 8 ½ x 11-in. or A4 paper) of the manuscript. A manuscript submission form should accompany the manuscript.

Tables and figures should be separate from the manuscript copy and only high-quality figures will be published. Figures should be original line art or glossy photos. Special instructions are required if figures are submitted by electronic means. To receive complete instructions and the manuscript submission form, please contact the Peer Review Coordinator, Erin Adams, at (305) 443-9353, ext. 275; FAX 305-443-7404; or write to the American Welding Society, 550 NW LeJeune Rd., Miami, FL 33126.